Helmut Elsenbeer, Keith Cassel, Jorge Castro

Spatial analysis of soil hydraulic conductivity in a tropical rain forest catchment

first published in:
Water Resources Research. - 28 (1992), 12, p. 3201 - 3214
ISSN: 0043-1397

Postprint published at the institutional repository of Potsdam University:
In: Postprints der Universität Potsdam :
Mathematisch-Naturwissenschaftliche Reihe ; 51
http://opus.kobv.de/ubp/volltexte/2008/1697/
http://nbn-resolving.de/urn:nbn:de:kobv:517-opus-16979

Postprints der Universität Potsdam
Mathematisch-Naturwissenschaftliche Reihe ; 51

WATER RESOURCES RESEARCH, VOL. 28, NO. 12, PAGES 3201–3214, DECEMBER 1992

Spatial Analysis of Soil Hydraulic Conductivity in a Tropical Rain Forest Catchment

HELMUT ELSENBEER

Institute of Geography, University of Berne, Berne, Switzerland

KEITH CASSEL

Department of Soil Science, North Carolina State University, Raleigh

JORGE CASTRO

Proyecto Suelos Tropicales, Lima

The topography of first-order catchments in a region of western Amazonia was found to exhibit distinctive, recurrent features: a steep, straight lower side slope, a flat or nearly flat terrace at an intermediate elevation between valley floor and interfluve, and an upper side slope connecting interfluve and intermediate terrace. A detailed survey of soil-saturated hydraulic conductivity (K_{sat})–depth relationships, involving 740 undisturbed soil cores, was conducted in a 0.75-ha first-order catchment. The sampling approach was stratified with respect to the above slope units. Exploratory data analysis suggested fourth-root transformation of batches from the 0–0.1 m depth interval, log transformation of batches from the subsequent 0.1 m depth increments, and the use of robust estimators of location and scale. The K_{sat} of the steep lower side slope decreased from 46 to 0.1 mm/h over the overall sampling depth of 0.4 m. The corresponding decrease was from 462 to 0.1 mm/h on the intermediate terrace, from 335 to 0.01 mm/h on the upper side slope, and from 550 to 0.015 mm/h on the interfluve. A depthwise comparison of these slope units led to the formulation of several hypotheses concerning the link between K_{sat} and topography.

INTRODUCTION

A state-of-knowledge report on tropical rain forest ecosystems [*UNESCO*, 1978] indicated a rather poor data base concerning the hydraulic properties of rain forest soils. It may be argued that this situation has improved since only marginally. While most of the new information on this topic concerns the soil surface or the uppermost soil layer [e.g., *Spaans et al.*, 1990; *Ghuman and Lal*, 1987], information about the spatial variability and depth functions of hydraulic properties is still scarce. In this latter respect, the only detailed information was provided by *Bonell et al.* [1983, 1987]. Their investigations involved the spatial coverage and sample sizes necessary for an assessment of the hydraulic conductivity-depth relationship and its spatial dependence.

The purpose of this study was to (1) investigate the relationship between saturated hydraulic conductivity (K_{sat}) and its changes with depth and topographic position by means of stratified sampling according to previously defined slope units, and (2) formulate hypotheses concerning this relationship to be tested on a regional scale.

RESEARCH SITE

The study catchment is situated in the Rio Pichis Valley in the Selva Central of Peru (75°5'W, 10°13'S). This area belongs to the western part of the Amazon Basin. The Rio Pichis forms part of the Pachitea drainage system which itself is part of the Ucayali basin (Figure 1). The geologic history of this area is described by *Kummel* [1948], *Ruegg* [1952] and *Koch* [1959]. These authors inferred an Ucayali peneplain to have formed after the latest Andean uplift during the later Tertiary [*Guizado*, 1975; *Dalmayrac et al.*, 1980]. Today, few remnants of that peneplain are discernible. Detailed topographic work by *Koch* [1959] revealed, instead of a uniform surface, a series of platforms the highest of which corresponds to the Ucayali peneplain. These platforms, or terraces, are well known throughout the upper Amazon Basin, and are referred to by the inhabitants of this region in specific vernacular terms [*Vidal*, 1987].

The change in fluvial regime, from depositional to erosional, resulting in the dissection of this peneplain, must have occurred in the Pliocene, according to the above authors. It is attributed to continual episodes of uplifting and/or subsidence. The field evidence for this tectonic activity, cited by these authors, includes entrenched stream meanders, dissection of the highest platforms, and headward growth of small tributaries. Recent side-looking airborne radar (SLAR) imagery of the Ucayali basin also has provided evidence for adjustments of the fluvial system due to tectonic activity [*Räsanen et al.*, 1987]. We were able to discern three platforms in the Rio Pichis Valley. The first and lowest platform corresponds to the Rio Pichis floodplain, about 5 m above low-flow stage. An escarpment of about 8 m separates the second platform from the floodplain. This platform is undulating and drained by incised streams. The degree of dissection is minor. The third and highest platform is about 15–20 m above the second one. In some places it is reduced to very narrow interfluves; in others more extensive, nearly

Paper number 92WR01762
0043-1397/92/92WR-01762$05.00

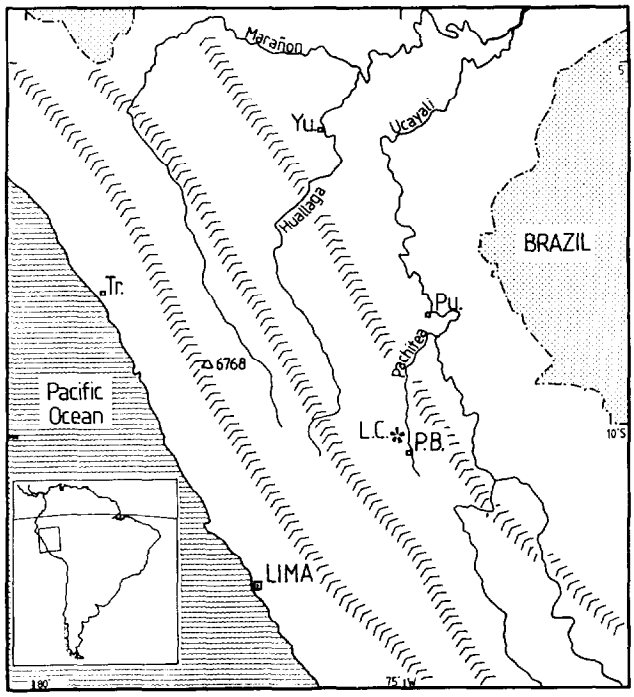

* L.C.: La Cuenca Research Station;
P.B.: Puerto Bermudez; Pu.: Pucallpa; Tr.: Trujillo; Yu.: Yurimaguas

Fig. 1. The location of the research catchment La Cuenca in Peru.

level areas are preserved. The generally convexolinear side slopes may reach 35°. The research catchment La Cuenca is located on this platform (Figure 2). Its prominent features are a narrow valley floor, the absence of concave foot slopes linking side slopes and valley floor, an intermediate, nearly flat terrace between an upper slope reaching the interfluve and a much steeper lower slope reaching the valley floor, and the presence of rills and gullies. Slope unit B corresponds to the lower slope, slope unit C to the intermediate terrace, slope unit D to the upper slope, and slope unit E to the interfluve (Figure 2). The following sequence of catchment development was deduced: (1) a gully stage as one end-member, at which a catchment consists of a steep gully with no indication of a valley floor, incising in slope unit B, (2) an intermediate stage where steep headwater gullies and a stream in a nearly flat valley floor are clearly discernible, and where slope unit C is still preserved, (3) a final stage in which poorly defined stream channels drain wide headwater swamps with low divides; at that stage, slope unit C is no longer discernible. Steep slope angles are maintained through all stages.

The research catchment represents an intermediate stage of catchment development, and thus displays the most complex topography to be expected in the above sequence, and hence also all possible topographic features: slope unit B exists at all stages, but is best developed in the intermediate stage, and can no longer be distinguished from slope unit D at the final stage; slope unit C has disappeared at the final stage, and units D and E may be difficult, if not impossible to distinguish at that stage. Thus, the research catchment, while definitely representative of the intermediate stage as outlined above, may also represent all possible slope units that are characteristic of this dissected regional platform.

Ultisols [*Soil Survey Staff*, 1975] are the dominant soil order in the Rio Pichis Valley [*Oficina Nacional de Evaluación de Recursos Naturales*, 1981], in accordance with their extensive occurrence in western Amazonia [*Buol et al.*, 1989]. They cover the above described platforms 2 and 3, while Entisols are common on platform 1, the Rio Pichis floodplain.

Within the research catchment, Ultisols are found on slope units C, D, and E (Figure 2), while an Inceptisol is associated with the steep slope unit B.

The research catchment is covered by primary rain forest. It belongs to a forest reserve, and to the best of our knowledge, it has not been affected by human intervention.

METHODOLOGY

Determination of K_{sat}

Undisturbed 0.076 by 0.076 m core cylinders were removed with a Uhland sampler, according to the stratification described above. On each slope unit, two 5 by 5 m plots were subdivided into 25 sections of 1 m^2. From each 1-m^2 section, three undisturbed core samples were taken at subsequent 0.1 m intervals. In addition, five cores per section were taken from the 0.3–0.4 m interval. On slope units C and D, a third 5 by 5 m plot was sampled to a depth of 0.2 m. This sampling scheme amounted to 740 undisturbed cores; the actual number of cores taken was considerably larger, for not every 1-m^2 section yielded a core deemed "undisturbed" at each depth interval at the first attempt. Table 1 summarizes the sampling procedure.

We considered the described sampling of 0.1 m depth increments the highest resolution attainable with the use of 0.076 by 0.076 m core cylinders. As some disturbance of the underlying layer was inevitable when removing a core, a depth increment corresponding precisely to the length of the core cylinder could not be realistically achieved. Hence, we assume that each core sample represents a 0.1 m depth increment. A relation to a particular soil horizon is not implied.

K_{sat} was determined, on core samples deemed undisturbed, by the constant head method [*Klute and Dirksen*, 1986], after a saturation period of 48 hours. The water temperature fluctuated between 24°C and 28°C, with occasional extremes as high as 30°C and as low as 22°C.

The greatest possible error associated with each determination of K_{sat} can be expressed as the sum of the errors of the individual measurements involved. The employed method is based on Darcy's law which for this purpose can be expressed as

$$\frac{V}{At} = K\frac{H}{l}, \qquad (1)$$

where V is the volume of water that passes through a sample of length l and a cross-sectional area A per time t due to hydraulic gradient H. The following possible measurement errors (pe) were considered: In V, if $V > 1000$ mL, then pe = 10 mL; if $100 < V < 1000$ mL, then pe = 5 mL; if $10 < V < 100$ mL, then pe = 1 mL; and if $V < 10$ mL, then pe = 0 mL. In H, pe = 1 mm. In l, pe = 2 mm. In A, there is no pe. In t, if $t < 100$ min then pe = 0.1 min; otherwise, pe = 0. The difference in possible measurement errors of V results from the use of different cylinders, with different graduations according to the respective percolation rate. The maximum possible error can be expressed as

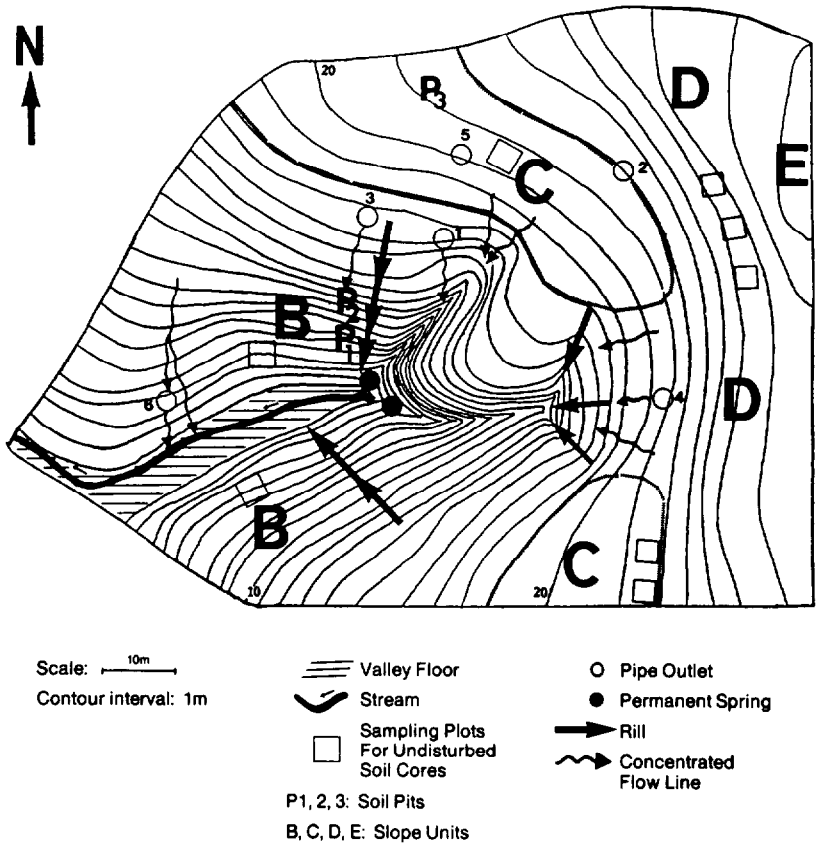

Fig. 2. The research catchment La Cuenca. The location of the sampling plots for undistributed soil cores on slope unit E is omitted for the sake of clarity.

$$dK = \frac{Vl}{HtA}\left(\frac{dV}{V} + \frac{dl}{l} - \frac{dt}{t} - \frac{dH}{H} - \frac{dA}{A}\right) \quad (2)$$

The error is greatest if the errors in V and l have the same sign, but the opposite of the errors in t and H. On the average, a maximum possible error of 5% was calculated. The actual error is probably less, so that the measurement accuracy is at least 95%.

Data Analysis

We attempted to approach the data set for this observational study without any a priori assumptions concerning underlying distributions. Although we certainly were aware of investigations, such as those by *Rogowski* [1972] and *Nielsen et al.* [1973], which support the assumption of a lognormal distribution of hydraulic conductivity data, we preferred to conduct the data analysis in a fashion as unbiased as possible. To this end, two broad phases of data analysis were distinguished: exploratory data analysis (EDA) and confirmatory data analysis (CDA). EDA reveals the structure of the data and its agreement, or lack thereof, with familiar models, which are often tacitly assumed; it should, however, precede any choice of a model. EDA provides evidence with is then evaluated by CDA. To paraphrase *Tukey* [1977], detective work (EDA) is required, before a judgment (CDA) can be made. *Tukey* [1977], *Mosteller and Tukey* [1977], and *Hoaglin et al.* [1983] provide an extensive array of EDA techniques. In the following, the tools employed in this study are briefly reviewed; the reader interested in details of these techniques, and of the underlying philosophy, is referred to the above authors.

TABLE 1. Number of Soil Samples for Each Unit and Depth

Slope Unit	0–0.1 m	0.1–0.2 m	0.2–0.3 m	0.3–0.4 m
B	50	50	50	10
C	75	75	50	10
D	75	75	50	10
E	50	50	50	10
Total	250	250	200	40

EDA

The techniques employed in this study are based on the concept of letter values [*Hoaglin*, 1983, p. 35]. These letter values are used to define resistant summary statistics which replace the classical summary statistics sample mean and sample variance as estimators of location and spread, respectively. Since exceptional values may have a drastic effect on the sample mean and a catastrophic effect on the sample variance, these two statistics might be misleading unless there is a priori knowledge about an underlying distribution. We did not assume this knowledge, and, hence, used resistant summaries, in accordance with the philosophy of EDA.

Letter values can be extracted from the data by sorting and ranking. After sorting a batch of data in ascending order, the rank of a particular observations can be defined by

counting up from the smallest value, or by counting down from the largest. That is, each observation is assigned an upward rank and a downward rank, and the following relationship holds: upward rank plus downward rank equals $n + 1$, where n is the number of observations in a batch.

By defining the depth of an observation in a batch as the smaller of its upward and downward rank, various summary values can be extracted from the data based on this concept.

The well-known median (M) has a depth of $(n + 1)/2$; if n is even, e.g., $n = 2k$, then, by convention, it falls halfway between the middle two observations of the ordered batch:

$$\text{median} = (x_{(k)} + x_{(k+1)})/2 \tag{3}$$

The extremes are the two observations with depth 1.

Additional pairs of summary values can be obtained by applying the rule

$$(\text{previous depth} + 1)/2$$

and starting with the median and its depth.

This procedure yields first the fourths (or "hinges" in Tukey's terminology) according to

$$\text{depth of fourth} = (\text{depth of median} + 1)/2 \tag{4}$$

The fourths essentially correspond to the quartiles; they encompass the middle half of a batch.

Applying this rule once more yields the eighths, according to

$$\text{depth of eighth} = (\text{depth of fourth} + 1)/2 \tag{5}$$

If any of the "previous depth" computations involves a fraction, this fraction is dropped before adding 1 and dividing by 2.

Depending on the size of a batch, one may continue to obtain additional pairs of summary values, such as the sixteenths, and so forth, until reaching the depth of 1 (the extremes).

The summary values arrived at in this fashion are assigned one-letter tags, for ease of notation and display: median, M; fourth, F; eighth, E; sixteenth, D; thirty-second, C; etc.

This scheme is based on the fact that E immediately precedes F, and uses the alphabet backward from F on and wrapping around so that Z follows A. In this way, the one-letter tags serve as mnemonic devices, and the associated summary values are now known as letter values.

A five-number summary, consisting of the median, the fourths, and the extremes, provides sufficient information about a batch of data. Additional letter values yield more details, if the batch under consideration is large enough. The flexibility of letter values makes these summaries a powerful tool for a preliminary assessment of the shape of the data.

Another resistant estimator of location, in addition to the median, is easily derived from a five-number summary. The trimean (TRI) is defined by:

$$\text{trimean} = (\text{lower fourth} + 2 \times \text{median} + \text{upper fourth})/4 \tag{6}$$

In contrast to the median, the trimean includes information about a batch farther from the center. In a symmetric batch, both estimators yield the same location estimate (and coincide with the sample mean if the batch has a Gaussian shape). Although both estimators are insensitive to a few large deviations in the data, the numerical value of the median is determined by only one or two of the central observations of a batch. Thus, small errors in these central observations, resulting from rounding, affect the median sharply [*Rosenberger and Gasko*, 1983, p. 314]. To account for this possibility, the trimean is listed together with the median in the letter value summaries, where appropriate.

Additional indications of location can be derived simply by forming the average of two corresponding letter values, which is called midsummary.

$$\text{midF} = (F_U + F_L)/2, \qquad \text{midE} = (E_U + E_L)/2, \text{ etc.} \tag{7}$$

where the subscripts U and L stand for upper and lower, respectively. These midsummaries contain evidence of systematic skewness in a bath [*Emerson and Stoto*, 1983, p. 105]. In a perfectly symmetric batch, all midsummaries coincide with the median. An increasing trend in the midsummaries reflects right skewness, a decreasing trend left skewness. If skewness is caused by a few exceptional values, only the more extreme midsummaries, say midC or midB, would be affected.

The previous discussion emphasized summaries of location. The same letter values may be used to summarize another important aspect of the data, their spread. "Spread" is a vague concept in the sense of *Mosteller and Tukey* [1977, p. 48] in contrast to a definite concept like the standard deviation. In EDA, the vague concept, derived from the data themselves without any additional assumptions, gives us the clues necessary to identify the corresponding definite concept for later use in confirmatory data analysis.

A simple resistant measure of spread is the fourth spread (d_F) where

$$d_F = \text{upper fourth} - \text{lower fourth} \tag{8}$$

This measure essentially corresponds to the interquartile range.

In analogy to d_F, one may define the eighth spread (d_E) and all the subsequent ones until arriving at the range which is the spread between the extremes. In contrast to the sample standard deviation or the range, the fourth spread in particular reflects the bulk of the data while being little affected by exceptional values ("outliers").

The spreads serve various useful purposes. The fourth spread, in particular, provides a means for identifying exceptional values. Certain outside cutoffs can be defined with d_F as a measure of distance. Outside values are those observations which are outside of the cutoffs defined by $F_L - 1.5d_F$ and $F_U + 1.5d_F$. Outside values defined in this fashion are not necessarily true "outliers"; they may well have the same behavior as the bulk of the data, but may be very unlikely if the data are assumed to follow a certain distribution.

The spreads also provide a first indication of how the data depart from the Gaussian shape as a familiar reference standard. For this purpose, the spread values of the data are divided by the corresponding Gaussian reference values (see, for example, *Velleman and Hoaglin* [1981, p. 53]): data $d_F/1.349$ ("F pseudosigma"); data $d_E/2.301$; data $d_D/3.068$; etc.

If the batch under consideration resembles a Gaussian sample, the quotients will vary little. An increasing trend in

the quotients indicates heavier tails than would be expected from a Gaussian shape, whereas a decreasing trend implies lighter tails. One has to keep in mind, of course, that the sensitivity to extreme values increases going from d_F to d_E and further. The plotting techniques suggested by *Hoaglin* [1985, p. 448] organize the information contained in the midsummaries, spreads, and pseudosigmas in an immediately comprehensible fashion. If a plot of midsummaries versus the corresponding spreads, or versus the square of the corresponding Gaussian quantiles, deviates from a horizontal line through the median, skewness is indicated. If a plot of pseudosigmas versus the square of the corresponding Gaussian quantiles deviates from a horizontal line, nonneutral elongation is indicated.

In conclusion, a set of letter values, and values derived from them, reveal a great deal about the structure of a batch by providing information about its location, spread, symmetry or lack thereof, tail length, and outside values.

The five-number summary of a batch of data, consisting of K_{sat} values for a given depth/slope unit combination, was displayed as a box plot [*Tukey*, 1977; *Emerson and Strenio*, 1983; *McGill et al.*, 1978], a graphical display of the essential features of a batch. The median is represented by the crossbar of the box plot, the upper and lower fourths by the ends of the box, and the two extremes by the two circles furthest from the box (see, for example, Figure 3). A line extending from each end of the box (the whiskers) reaches as far as the outside cutoffs. The length of the box, then, is an indication of the spread, the measure of spread being the fourth spread. Since the box plot is based on resistant measures of location and spread, it is itself resistant, and reflects the structure of the actual data, not that of an assumed underlying distribution. It summarizes the data in a compact fashion. Box plots are particularly useful for comparing several batches, e.g., several slope units for a given depth interval (see Figures 3–6). They also give a first clue as to the next step in data analysis, which may be confirmed by looking at the two diagnostic plots based on midsummaries and pseudosigmas.

Inspection of these diagnostic plots supports any decision based on box plots as to whether one may proceed with CDA, and with which estimators, or whether reexpression in a different scale is required before proceeding with CDA. In this study, the previously described techniques are repeated for each of the four selected reexpressions: square root (not included in the results because of its ineffectiveness), cube root, fourth root, and logarithmic.

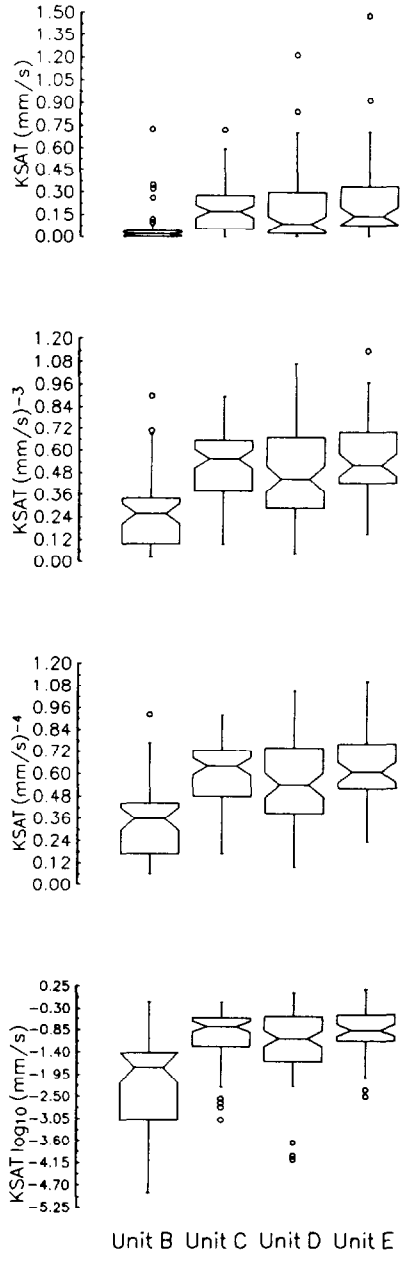

Fig. 3. The effect of transformations on the batches from the depth interval 0–0.1 m. The ends of each box correspond to the upper and lower fourth, the crossbar to the median of a batch. The lines extending from each end of the box indicate the outside cutoffs; outside values are represented by circles. The length of each box reflects the fourth spread, or interquartile range. See text for definitions of terms.

CDA

Confirmatory data analysis begins with evaluating the evidence from EDA concerning Gaussian shape before and after data transformation. Confirmation is based on a test proposed by *Martinez and Iglewicz* [1981], which involves robust estimators of location and scale [*Iglewicz*, 1983, p. 425]. If Gaussian shape is ascertained by this test, CDA proceeds with the calculation of classical confidence intervals based on the arithmetic mean and the standard deviation; in the face of non-Gaussian behavior robust confidence intervals are calculated. For the sake of comparison, both types of confidence intervals are reported.

Robust confidence intervals involve robust estimators of location and scale. We used several M estimators to minimize objective functions, according to *Huber* [1964]:

$$\sum_{i=1}^{n} \rho(x_i, t) \text{ min!} \tag{9}$$

where x_i denotes each observation and t the estimate. If ρ has a derivative $\psi(x, t) = \partial[\rho(x, t)]/\partial t$ then T_n is that value of t that satisfies the equation

$$\sum_{i=1}^{n} \psi(x_i, t) = 0. \tag{10}$$

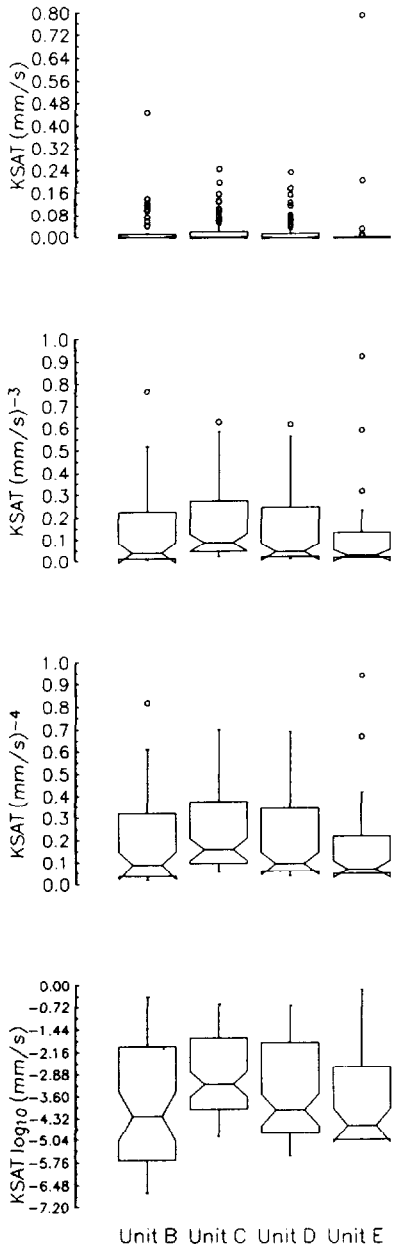

Fig. 4. Same as Figure 3, except for the depth interval 0.1–0.2 m.

The choice of ψ determines a specific M estimator.

In addition, an alternative form of M estimation known as W estimation was employed [*Goodall*, 1983, p. 381]. If the M estimate T_n is defined by

$$\sum_{i=1}^{n} \Psi\left(\frac{x_i - T_n}{cS_n}\right) = 0 \tag{11}$$

and the weight function w according to $uw(u) = \psi(u)$, then the W estimate is defined by:

$$\sum_{i=1}^{n} \left(\frac{x_i - T_n}{cS_n}\right) w \left(\frac{x_i - T_n}{cS_n}\right) = 0 \tag{12}$$

with

$$u_i = (x_i - T_n)/(cS_n) \tag{13}$$

where c is a tuning constant and S_n is a robust estimate of scale.

Both M and W estimates are calculated iteratively, the former by the Newton-Raphson algorithm. A suitable starting value for T_n is the median, because of its resistance. As scale estimate S_n we used the median absolute deviation from the median (MAD) [*Hoaglin et al.*, 1983, p. 291], defined as

$$\text{MAD} = \text{median}\ (|x_i - \text{median}\ (x_i)|) \tag{14}$$

The rule that in most situations the W estimate is the same as the M estimate [*Goodall*, 1983, p. 385], and specifically, that the one-step W estimate is as good as the fully iterated M estimate [*Hoaglin et al.*, 1983, p. 293], applied in this

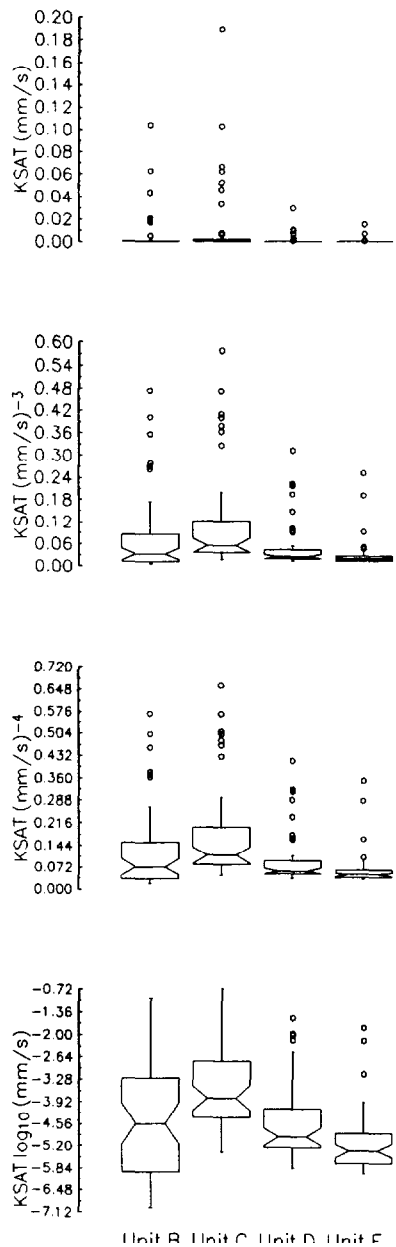

Fig. 5. Same as Figure 3, except for the depth interval 0.2–0.3 m.

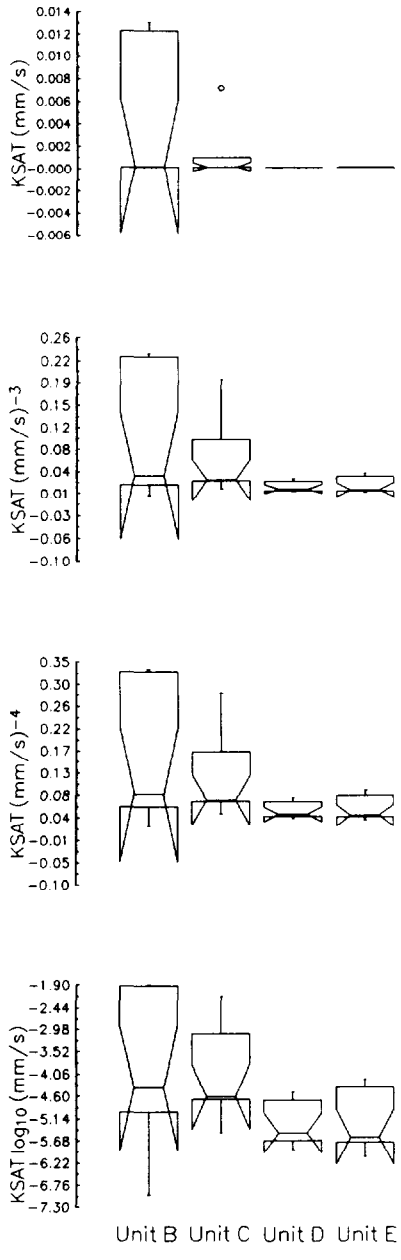

Fig. 6. Same as Figure 3, except for the depth interval 0.3–0.4 m.

study as well. Therefore, only the W estimates based on the biweight (see below) are reported. Table 2 summarizes the estimators used in this study.

The choices of tuning constants were $c = 9$ and $c = 6$ for the biweight estimator [*Mosteller and Tukey*, 1977, pp. 205, 235], and 2.4π and 2.1π for the wave estimator [*Andrews et al.*, 1972].

In order to calculate confidence intervals for the above location estimates, robust scale estimates are required. We employed A estimators of scale which have the general form [*Iglewicz*, 1983, p. 416]

$$s_T = \frac{(c \text{ MAD}) \sqrt{n} \left[\sum_{i=1}^{n} \psi^2(u_i) \right]^{1/2}}{\left| \sum_{i=1}^{n} \psi'(u_i) \right|} \tag{15}$$

Specifically, the ψ functions listed in Table 2 were used.

The choice of t values for the construction of confidence intervals is based on *Iglewicz* [1983] and *Gross* [1976]. As the results for the wave-based and biweight-based estimates were nearly identical, only the latter are reported. In addition, the confidence intervals based on the arithmetic mean and standard deviation, and those based on the median and fourth spread, are listed in Table 3. The definitions of the statistics used are summarized in Table 4.

The calculation of confidence intervals concludes the data analysis; the conclusions based on EDA are either confirmed or contradicted, and hypotheses concerning the link between K_{sat} and topographic position on a larger scale may be formulated.

The SAS language and procedures were used for all calculations [*SAS Institute, Inc.*, 1988*a*, *b*].

Results and Discussion

The various steps of data analysis as outlined in the previous section generated a large amount of numerical and graphical information. In the following, we illustrate the decision-making process in detail for one slope unit, C, only, and report for the remaining slope units the outcome of the analysis without detailed numerical and graphical documentation.

Exploratory Data Analysis

Slope unit C. Figure 7 displays a monotonically increasing trend in the midsummaries of the original data for the 0–0.1 m depth. This trend is practically eliminated by reexpression in the fourth root and cube root scale. The log transformation results in a monotonically decreasing trend, i.e., right skewness is replaced by left skewness. These effects are also obvious from Figure 3. The pseudosigmas (Figure 8) are quite stable in all scales. The asymmetry introduced by the log transformation is reflected in a mean smaller than the median, in the original scale, the opposite holds true (Table 5). Again, the results from the diagnostic plots are confirmed.

Figure 9 shows a strong trend in the midsummaries for the 0.1–0.2 m data which is not alleviated entirely by any of the transformation. Reexpression in the log scale appears to have the strongest effect on removing this trend. This conclusion is supported by Figure 4: In the log scale, the

TABLE 2. Estimators and Their Pertinent Functions

Estimator	Objective Function	Ψ Function	Weight Function
Tukey's biweight	$(1/6)[(1-(1-u^2)^3]$	$u(1-u^2)^2$	$(1-u^2)^2$
Andrew's sine wave	$(1/\pi)(1-\cos \pi u)$	$(1/\pi)(\sin \pi u)$	$(1/\pi u)(\sin \pi u)$

TABLE 3. Location Estimates and 95% Confidence Intervals for K_{sat} Values Based on the Arithmetic Mean and Standard Deviation, and the Median and Fourth Spread, Respectively

Slope Unit	Estimator	Lower Limit	Location Estimate	Upper Limit
		0–0.1 m Depth		
B	mean	66	135	249
	median	88	164	283
C	mean	915	1229	1618
	median	1151	1493	1907
D	mean	649	944	1330
	median	578	829	1153
E	mean	1073	1556	2184
	median	955	1363	1890
		0.1–0.2 m Depth		
B	mean	0.3	1.2	4.4
	median	0.2	0.6	1.9
C	mean	6.3	12.4	24.1
	median	2.7	5.0	9.4
D	mean	1.8	4.2	9.7
	median	0.4	0.9	2.0
E	mean	0.4	1.0	2.4
	median	0.1	0.3	0.6
		0.2–0.3 m Depth		
B	mean	0.1	0.27	0.82
	median	0.1	0.27	0.76
C	mean	1.4	3.0	6.7
	median	0.7	1.5	3.1
D	mean	0.14	0.28	0.56
	median	0.06	0.11	0.22
E	mean	0.005	0.009	0.015
	median	0.003	0.004	0.008
		0.3–0.4 m Depth		
B	mean	0.03	0.42	6.21
	median	0.03	0.41	4.99
C	mean	0.09	0.45	2.39
	median	0.05	0.25	1.15
D	mean	00.02	0.04	0.09
	median	0.02	0.03	0.07
E	mean	0.002	0.005	0.014
	median	0.001	0.003	0.007

All values are in the original scale, in units of 10^{-4} mm s^{-1}.

whiskers are of nearly equal length, and the median line approaches the middle of the box compared to the other three transformations. Figure 10 reveals that the transformations result in lighter than neutral tails. The skewness persisting after reexpression is reflected in means larger than trimeans which, in turn, are larger than the medians (Table 5). The discrepancy between the estimates based on these estimators is smallest for the log transformation.

Figure 11 clearly reveals an apparent near-Gaussian behavior in the middle of the untransformed batch data for 0.2–0.3 m depth. Consequently, the midsummaries of the transformed batches show the strongest trend in this portion, whereas they level off in the tails. This unusual behavior is also reflected in the discontinuous trend of the pseudosigmas (Figure 12), as well as in Table 5. Here, as was the case of the 0.1–0.2 m depth increment, the relative values of the mean, trimean, and median reflect the asymmetry in the middle portion. The discrepancy is least in the case of the log transformation. The visual display of Figure 5 also supports the choice of this transformation: The position of the median line indicates somewhat asymmetrical conditions in the middle of the batch, but the relative length of the whiskers and the absence of outside values demonstrate near overall symmetry.

No transformation results in a good agreement of mean, trimean, and median for the 0.3–0.4 m data (Table 5). Both root transformations seem to promote symmetry in the middle of the batch, whereas the log transformation promotes overall symmetry. The latter interpretation is also supported by Figure 6.

In summarizing these results for slope unit C, we find that while symmetry is successfully promoted by either of the root transformations in the batch from depth 0–0.1 m, none of the transformations seems entirely appropriate for the batches from the lower depth intervals. In those, reexpression in the log scale appears to alleviate asymmetry more than the other options.

Slope unit B. Similar to slope unit C, an overall increasing trend in midsummaries and pseudosigmas of the original batch from the 0–0.1 m depth was observed. The underlying asymmetry persisted after both root transformations, which may be confirmed by inspecting Figure 3. Although reexpression in the log scale appears to promote overall symmetry, it introduces asymmetry in the middle portion of the batch. This dilemma was confirmed by the discrepancy between mean, median, and trimean.

The trend in pseudosigmas was removed after reexpression in any of the other scales, i.e., elongation was no longer a problem.

The diagnostic plots for asymmetry and elongation of the 0.1–0.2 m K_{sat} data suggested a behavior similar to the previous batch in that no one transformation deals effectively with both these aspects. In fact, the data in the original scale appear to be no more skewed than the reexpressed data, except for the very tail end. A comparison of mean, median, and trimean reflected the unresolved situation. As before, log transformation was selected as a compromise. Judging by the box plots alone (see Figure 4), the log scale definitely performs better than any other scale.

As occurred for the previous two batches, the log transformation of the data for the 0.2–0.3 and 0.3–0.4 m depths was selected in the face of an inconclusive situation, espe-

TABLE 4. Estimators and Confidence Intervals Used in the Present Study

Estimator	Symbol	Confidence Intervals
Mean	$\bar{x}$	$\bar{x} \pm (t_{n-1}s)n^{-1/2}$
Standard deviation	s	
Median	M	$M \pm [t_{n-1}(d_F)]\,(1.075\,n^{1/2})^{-1}$
Fourth spread	d_F	
One-step W estimator based on biweight	T_b	$t_{0.7\,(n-1)}\,S_b n^{-1/2}$
A estimator based on biweight	s_b	

cially for depth interval 0.2–0.3 m. In this case, the box plot display (Figure 5) favors reexpression in the log scale. For the depth interval 0.3–0.4 m, a transformation does not appear necessary (Figure 6). It must by kept in mind, however, that the small sample size limits the usefulness of the graphical display.

When considering slope unit B as a whole, none of the transformations employed appears successful in promoting symmetry or neutral elongation in any of the batches, with the possible exception of depth interval 0.3–0.4 m.

Slope unit D. The diagnostic plot for asymmetry of K_{sat} data in the 0–0.1 m depth suggested that the lack of symmetry in the original data is efficiently removed by the root transformations, whereas reexpression in the log scale failed in the tails. Figure 3 confirms this interpretation. Reexpression in the fourth root scale practically removed the slight trend in the pseudosigmas of the original data. Considering the middle portion only, the overall good performance of the fourth root transformation was supported by the best agreement between mean, median, and trimean.

The trend in midsummaries of the original data for the 0.1–0.2 m depth was not removed by any of the transformations. Outside of the fourth spread, reexpression in the log scale performed best. Accordingly, a discrepancy between median and trimean persisted after transformation. The difference between the respective estimates is least in the case of the log transformation. Figure 4 also supports this choice.

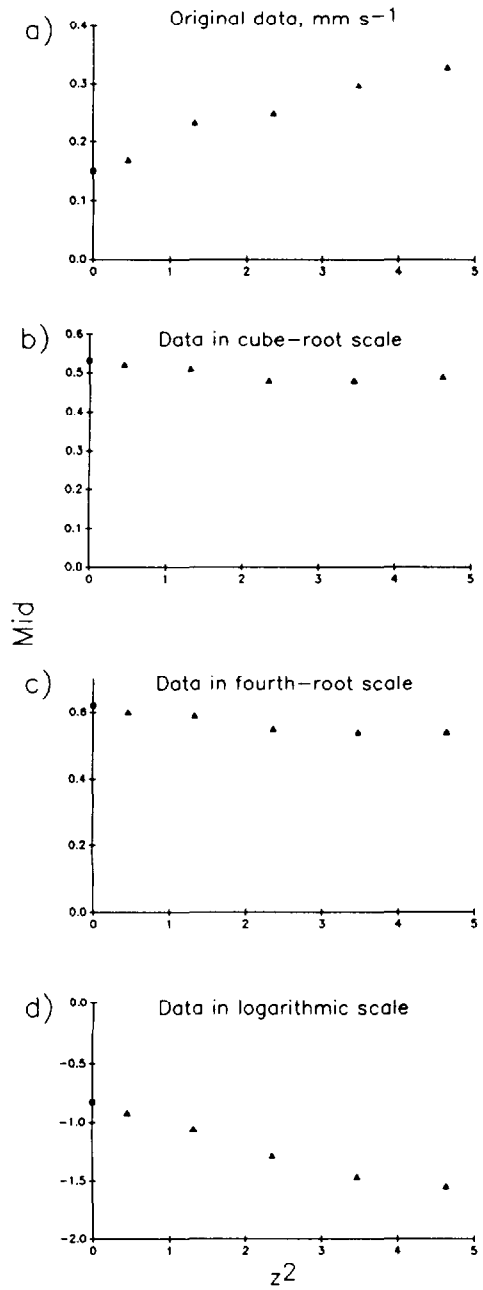

Fig. 7. Midsummaries versus z^2 plot of K_{sat} values from slope unit C, depth 0–0.1 m.

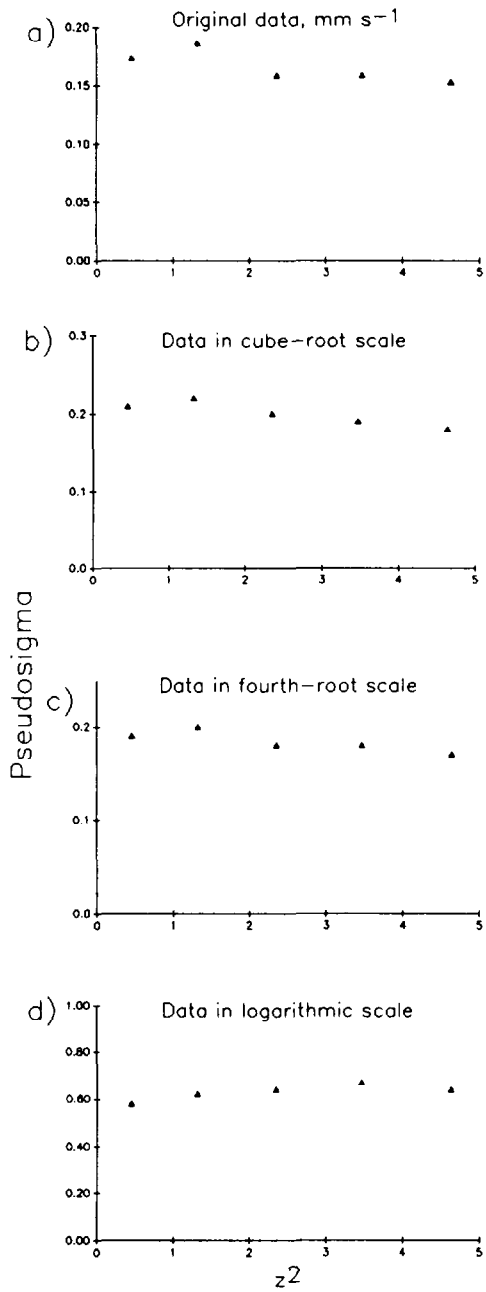

Fig. 8. Pseudosigma versus z^2 plot of K_{sat} values from slope unit C, depth 0–0.1 m.

TABLE 5. Comparison of the Effect of Transformations on Various Location Estimators for K_{sat} Values From Slope Unit C

Transformation	Mean	Median	TRI	T_b*
		0–0.1 m Depth		
None	0.14	0.05	0.16	0.07
Cube root	0.13	0.15	0.15	0.14
Fourth root	0.12	0.15	0.14	0.13
Logarithmic	0.10	0.15	0.13	0.12
		0.1–0.2 m Depth		
None	0.02187	0.00010	0.00574	0.00007
Cube root	0.00535	0.00054	0.00189	0.00073
Fourth root	0.00366	0.00050	0.00148	0.00095
Logarithmic	0.00124	0.00050	0.00086	0.00104
		0.2–0.3 m Depth		
None	0.00467	0.00001	0.00050	0.00001
Cube root	0.00142	0.00016	0.00029	0.00019
Fourth root	0.00091	0.00015	0.00025	0.00017
Logarithmic	0.00030	0.00015	0.00019	0.00023
		0.3–0.4 m Depth		
None	0.00066	0.00001	0.00003	0.00001
Cube root	0.00013	0.00003	0.00003	0.00003
Fourth root	0.000094	0.000025	0.000027	0.000024
Logarithmic	0.000045	0.000025	0.000013	0.000029

All estimates are in the respective reexpressed scale. Values are in units of millimeters per second.
*Based on tuning constant $c = 9$.

A strong asymmetry was evident from the respective diagnostic plot of the data from the 0.2–0.3 m depth, which was not entirely removed by any of the transformations. The strong effect of the tails, however, was practically neutralized by the log transformation. The good agreement between the mean, trimean, and median supported the choice of that transformation. This effect of the log transformation is displayed in Figure 5. The diagnostic plot for elongation indicated near-neutral tails in the case of reexpression in the log scale.

All transformations promoted symmetry for the 0.3–0.4 m depth. As before, the log transformation was selected (see also Figure 6).

For slope unit D as a whole, the root transformations are appropriate for the batch from the 0–0.1 m depth interval, whereas the log transformation, though not entirely satisfactory, provides an improvement over the original scale for the batches from the subsequent depth intervals.

Slope unit E. The diagnostic plots of the 0–0.1 m data depicted a situation similar to the previous slope units. The increasing trend in midsummaries of the original batch was effectively removed by the fourth root transformation, whereas the log transformation merely reversed the asymmetry. Reexpression in the fourth root scale also stabilized the trend in pseudosigmas, which is present in the original scale. Figure 3 supports these conclusions.

The diagnostic plots of data from the 0.1–0.2 m depth confirmed the previous conclusions about this depth interval: No transformation is satisfactory, but the logarithmic one offers the best solution. The trend in the midsummaries of the original data was very strong, implying considerable tail-heaviness. This was also reflected in the discrepancy between mean, median, and trimean. The log transformation reduced this discrepancy more than the root transformations. Figure 4 suggests the same conclusion.

Only a partial removal of the trend in midsummaries of the original data from the 0.2–0.3 m depth was achieved upon applying transformations. All three transformations promoted symmetry in the middle of the batch, as was documented by the good agreement between the median and the trimean. The discrepancy between the mean and these two resistant estimates, however, was smallest for the log transformation. This implies a smaller efficiency of the root transformations in the tails. As before, there is no ideal solution, but reexpression in the log scale seems to be the best one available. Figure 5 also supports this conclusion.

Both the log and the fourth root transformations appeared to promote symmetry of data at the 0.3–0.4 m depth, but no clear decision was possible. For easier comparison with the

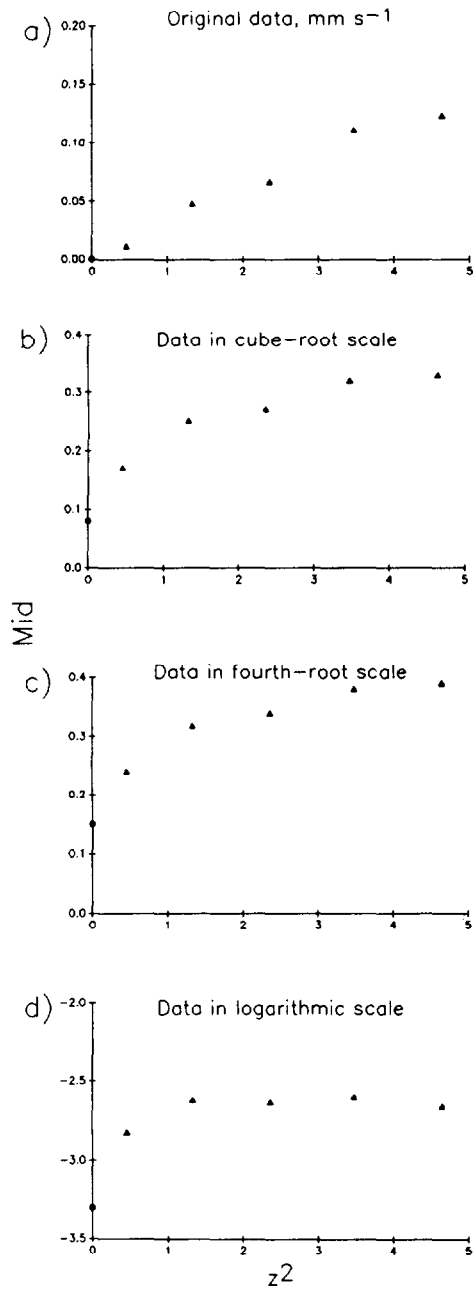

Fig. 9. Midsummaries versus z^2 plot of K_{sat} values from slope unit C, depth 0.1–0.2 m.

other batches from this depth interval, the log transformation was selected.

For slope unit E the fourth root transformation deals effectively with the asymmetry present in the batch from the uppermost depth interval. While not entirely satisfactory, the log transformation offers the best solution for the batches from the lower depth intervals.

Results of the exploratory data analysis allow several preliminary conclusions. K_{sat} decreases sharply with depth in all landscape positions, although the K_{sat}-depth functions themselves differ noticeably. Second, K_{sat} of the soil surface (depth 0–0.1 m) varies considerably among topographic positions. The differences, however, among slope units C, D, and E are much smaller than the differences between any of them and slope unit B.

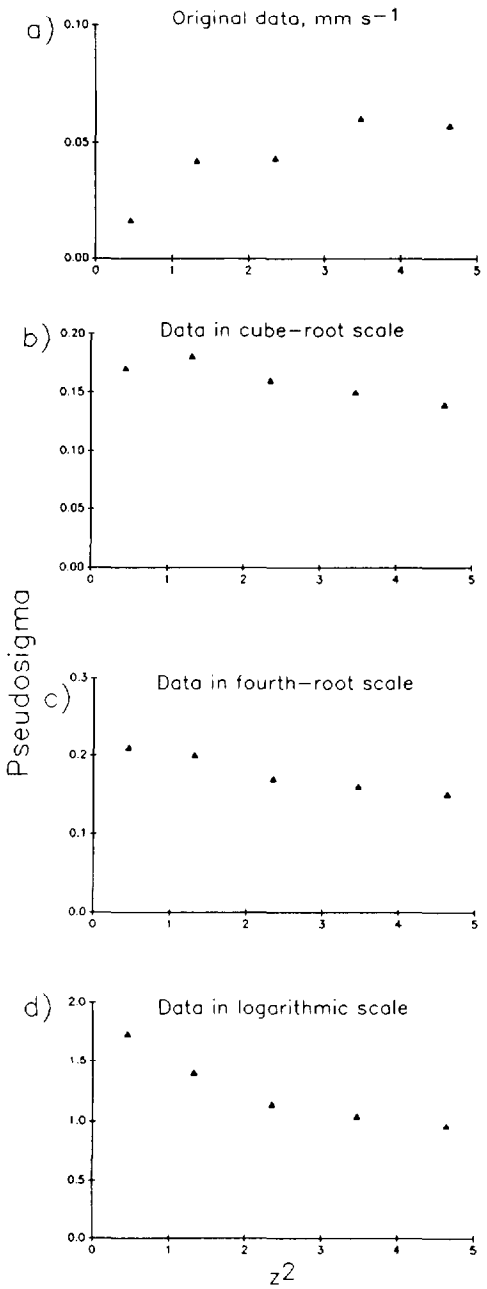

Fig. 10. Pseudosigma versus z^2 plot of K_{sat} values from slope unit C, depth 0.1–0.2 m.

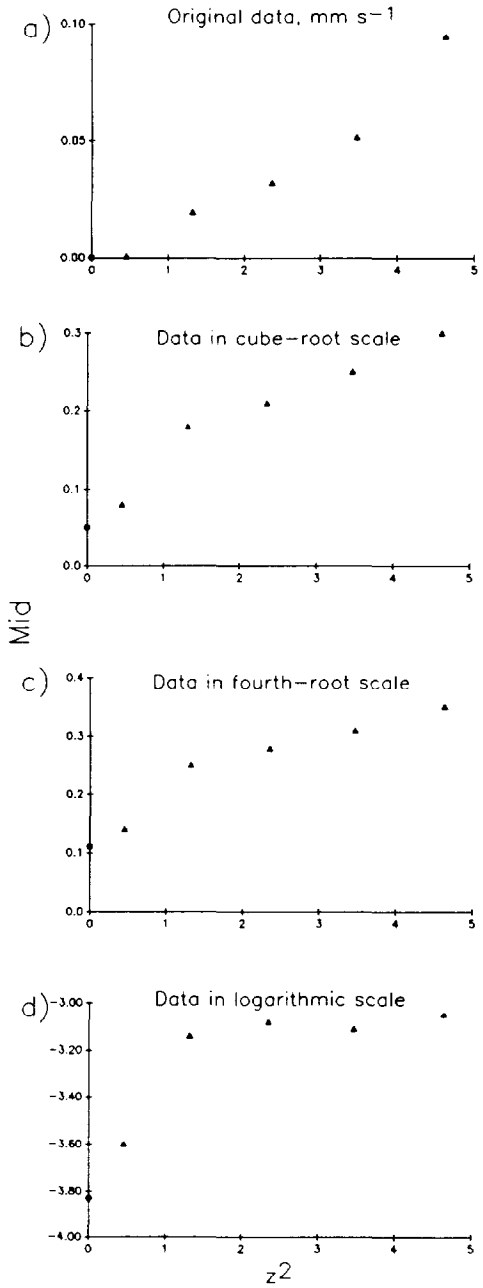

Fig. 11. Midsummaries versus z^2 plot of K_{sat} values from slope unit C, depth 0.2–0.3 m.

Finally, all batches display considerable skewness, regardless of landscape position and depth. This skewness is either partially or completely removed by root and log transformations for the uppermost and the lower depth intervals, respectively. Whether the differences between the topographic positions are significant, in the statistical sense, is the subject of the following.

Confirmatory Data Analysis

Slope unit C. The unsatisfactory outcome from EDA requires formal testing for departure from Gaussian shape

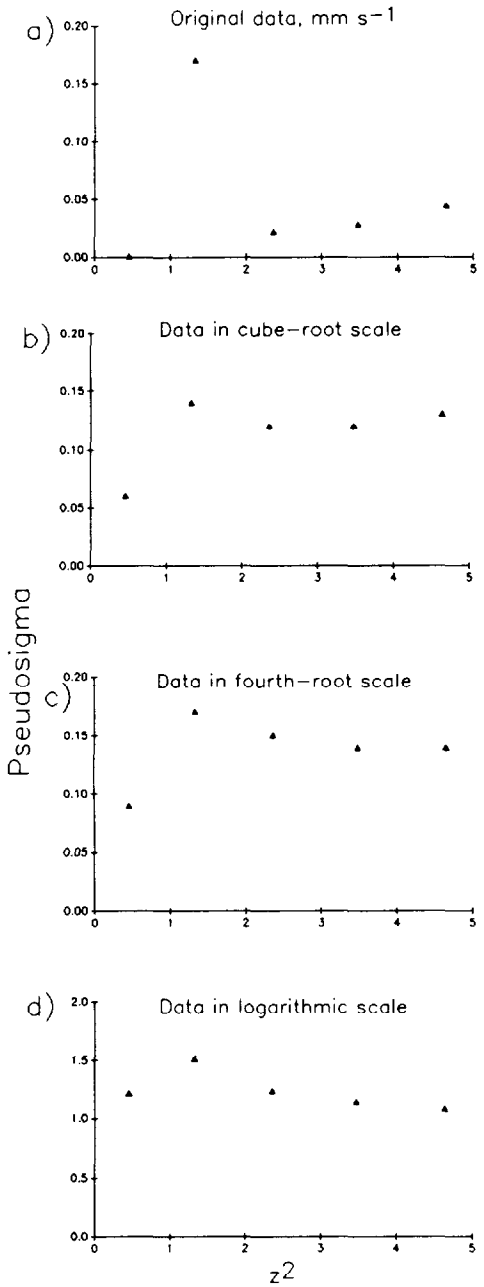

Fig. 12. Pseudosigma versus z^2 plot of K_{sat} values from slope unit C, depth 0.2–0.3 m.

before choosing location and scale estimators. The Martinez-Iglewicz I test is employed to test the hypothesis that the underlying distributions have a Gaussian shape after reexpression. Table 6 confirms the usefulness of the root transformations for the batch from depth interval 0–0.1 m, and points to the log transformation for the other batches. The test result itself would support the use of mean and standard deviation. As a precaution, however, the estimators based on the biweight are also employed. The location estimates are significantly different at the chosen confidence level, regardless of estimator or tuning constant, including the mean and median (see Table 7).

Table 8 displays the final location estimates based on the biweight estimators and the above suggested transformations. Expressed in easily understood units, K_{sat} decreases, first sharply and then gradually, from 462 to 3.7 to 0.8 to 0.1 mm/h over a depth interval of 0.4 m. The decrease in K_{sat} from the first to the second depth interval corresponds to 2 orders of magnitude.

Slope unit B. Contrary to what was indicated by EDA, log transformation resulted in Gaussian shape for batches from all four depth intervals, according to the I test. Fourth root transformation does the same for the batch from depth interval 0–0.1 m. This outcome does not depend on the choice of the value of c, the tuning constant, except for the cube root transformation of the data corresponding to the uppermost soil layer. In this case, the null hypothesis of Gaussian shape would have been accepted if the smaller value of 6 had been chosen as tuning constant. A smaller tuning constant means rejection of more outlying values. For this case, it implies that the center of the batch has Gaussian shape, but that the tails are nonneutral to the extent that the null hypothesis is rejected, unless the tails are shortened by a smaller c.

Table 8 displays the final location estimates based on the biweight estimator, the fourth root transformation for the depth interval 0–0.1 m, and the log transformation for all others.

K_{sat} of slope unit B decreases from 46 to 0.4 to 0.1 mm/h over a total depth of only 0.3 m. The location estimates from the lower two depth intervals are not significantly different, nor are those corresponding to the 0.1–0.2 m and 0.3–0.4 m intervals. This conclusion holds independent of the chosen estimator or tuning constant with the exception of the median, which did not recognize a significant difference between any of the lower three depth intervals.

Slope unit D. The test results generally supported the above interpretations from EDA. As before, fourth root transformation results in Gaussian shape for the data from the upper depth interval. Log transformation achieves the same for the data from the lower depth intervals, with the exception of 0.2–0.3 m, confirming the EDA result. The discrepancy between the mean and T_b in the third depth

TABLE 6. Martinez-Iglewicz' I Test for Departure From Gaussian Shape for K_{sat} Values From Slope Unit C

Transformation	I	P_{95}
	0–0.1 m Depth (n = 75)	
Cube root	0.876	
Fourth root	0.977	1.102
Logarithmic	1.359	
	0.1–0.2 m Depth (n = 75)	
Cube root	8.943	
Fourth root	2.123	1.102
Logarithmic	0.932	
	0.2–0.3 m Depth (n = 50)	
Cube root	23.614	
Fourth root	7.038	1.145
Logarithmic	1.066	
	0.3–0.4 m Depth (n = 10)	
Cube root	73.173	
Fourth root	10.836	1.962
Logarithmic	1.681*	

The significance level is $k = 0.05$; the tuning constant is $c = 9$.
*I statistics whose values would become smaller or larger than P_{95}, if the tuning constant $c = 6$ is selected for its calculation.

interval reflected the unusual situation and justified the use of a robust estimator. In all cases, the confidence intervals based on the mean were wider than the respective robust ones. All location estimates were significantly different, regardless of estimator or tuning constant.

Table 8 presents the results based on the biweight estimator and the same transformations as above. On slope unit D, K_{sat} decreases from 335 to 1.1 to 0.05 to 0.01 mm/h over 0.4 m.

Slope unit E. No significant departure from Gaussian shape was evident for the batch from the surface depth interval, irrespective of the transformation employed. Reexpression in the log scale does not promote Gaussian shape in the batches from the 0.1–0.2 m and 0.2–0.3 m depth intervals. This situation suggests the use of a robust location estimator.

Table 8 displays the final estimates based on the biweight, the fourth root and log transformation for the first and all subsequent depth intervals, respectively. The most conspicuous discontinuity between the first and second depth interval occurs on this slope unit. K_{sat} decreases from 550 to 0.2 mm/h over 0.1 m. Another decrease by 1 order of magnitude, to 0.02 mm/h, occurs in the next depth increment. The estimate of 0.015 mm/h for the depth 0.3–0.4 m is not significantly different from the one above it.

TABLE 8. Comparison of Slope Units by Depth With Respect to Location Estimates and 95% Confidence Limits for K_{sat} Values Based on T_b and s_b and the Tuning Constant $c = 9$

Slope Unit	Lower Limit	Location Estimate	Upper Limit
	0–0.1 m Depth		
B	61	127	237
C	949	1283	1699
D	628	929	1327
E	1037	1526	2170
	0.1–0.2 m Depth		
B	0.3	1.1	4.4
C	5.0	10.4	21.6
D	1.2	3.0	5.8
E	0.2	0.6	1.3
	0.2–0.3 m Depth		
B	0.08	0.25	0.81
C	1.0	2.3	5.3
D	0.09	0.15	0.25
E	0.004	0.005	0.008
	0.3–0.4 m Depth		
B	0.02	0.40	7.30
C	0.07	0.29	1.19
D	0.02	0.04	0.09
E	0.001	0.004	0.013

All estimates are in the original scale, in units of 10^{-4} mm s^{-1}.

Comparison of Slope Units by Depth and Formulation of Hypotheses

Depth 0–0.1 m. Figure 3 emphasizes the distinct nature of slope unit B.

The differences among the remaining slope units are comparatively minor. Table 8 suggests that based on T_b and the respective confidence limits, slope unit D has a significantly lower K_{sat} than slope unit E. The two nearly level slope units C and E are not different.

These results suggest the formulation of the following hypotheses concerning the surface hydrology of this rain forest environment: (1) Saturated hydraulic conductivity is lowest on the steep lower side slopes bordering the streams. (2) Level or nearly level portions of the landscape, regardless of relative elevation, have the same hydraulic conductivity. (3) Where an upper side slope can be identified, its K_{sat} is the same or lower than that of the level portions of the landscape, but higher than that of the steep lower side slopes.

TABLE 7. Final Location Estimates and 95% Confidence Limits for K_{sat} Values from Slope Unit C

Estimator	Lower Limit	Location Estimate*	Upper Limit
	0–0.1 m Depth		
Mean	915	1229	1618
T_b	949	1283	1699
Median	1151	1493	1907
	0.1–0.2 m Depth		
Mean	6.3	12.4	24.1
T_b	5.0	10.4	21.6
Median	2.7	5.0	9.4
	0.2–0.3 m Depth		
Mean	1.4	3.0	6.7
T_b	1.0	2.3	5.3
Median	0.7	1.5	3.1
	0.3–0.4 m Depth		
Mean	0.09	0.45	2.39
T_b	0.07	0.29	1.19
Median	0.05	0.25	1.15

All estimates are in the original scale, in units of 10^{-4} mm s^{-1}.
*Depth 0–0.1 m is based on fourth root transformation: the remaining depths, on logarithmic transformation.

Depth 0.1–0.2 m. Figure 4 suggests that slope unit C has the highest K_{sat} in this depth interval. Furthermore, all other slope units do not appear different. Table 8 supports the former conclusion, but points to a distinction among slope units B, D, and E. The following hypotheses concerning the 0.1–0.2 m depth interval should be considered: (1) Saturated hydraulic conductivity is highest on the intermediate terrace between valley bottom and interfluve. (2) Upper and lower side slopes have the same hydraulic conductivity. (3) The interfluves have the lowest K_{sat}.

Depth 0.2–0.3 m. Figure 5 clearly reveals the high K_{sat} of slope unit C. Slope unit E seems to have the lowest K_{sat}, while B and D might not differ significantly. Table 8 confirms these conclusions, which were not affected by the choice of the estimator, with one exception: The K_{sat} of slope units E and B did not differ if the comparison was based on the mean.

Three hypotheses may be formulated: (1) K_{sat} is highest on the intermediate terrace between valley bottom and interfluve. (2) K_{sat} is lowest on the interfluve. (3) Upper and lower side slopes have the same K_{sat}.

Depth 0.3–0.4 m. The enormous spread of the K_{sat} values from slope unit B (see Figure 6) renders a distinction of this unit from others nearly impossible. The K_{sat} of slope units B and C, and D and E, respectively, appear similar. In accordance with the estimates from Table 8, at least two hypotheses concerning the 0.3–0.4 m depth emerge: (1) The steep lower side slopes and the intermediate terraces have the same K_{sat}. (2) The interfluves have the lowest K_{sat}.

SUMMARY

A detailed survey of K_{sat} in a first-order rain forest catchment of western Amazonia revealed an obvious link between soil hydraulic conductivity and topographic position. The establishment of this link suggests several hypotheses whose testing would require sampling at the regional scale.

1. Surface K_{sat} is lowest on side slopes with active surficial processes; surface K_{sat} of level or nearly level portions of the landscape is the same regardless of their relative elevations above the valley floors. We attribute the higher surface K_{sat} of these topographic positions to the observed biotic activity which is undisturbed by surficial processes, in contrast to the lower side slopes.

2. K_{sat} decreases sharply with depth in all topographic positions, but the K_{sat}-depth functions themselves differ among these positions. The decrease in K_{sat} with depth is most pronounced on the interfluves.

3. Subsurface K_{sat} is highest on the intermediate terraces between valley floor and interfluve, and lowest on the interfluves.

REFERENCES

Andrews, D. F., P. J. Bickel, F. R. Hampel, P. J. Huber, W. H. Rogers, and J. W. Tukey, *Robust Estimates of Location: Survey and Advances*, Princeton University Press, Princeton, N. J., 1972.

Bonell, M., D. A. Gilmour, and D. S. Cassells, A preliminary survey of hydraulic properties of rainforest soils in tropical north-east Queensland and their implications for the runoff process, *Catena*, *4*(Suppl.), 57–78, 1983.

Bonell, M., D. S. Cassells, and D. A. Gilmour, Spatial variations in soil hydraulic properties under tropical rainforest in northeastern Australia, in *International Conference on Infiltration, Development and Application*, edited by Y. Fok, pp. 153–165, Water Resources Center, University of Hawaii, Hilo, 1987.

Buol, S. W., F. D. Hole, and R. J. McCracken, *Soil Genesis and Classification*, Iowa State University Press, Ames, 1989.

Dalmayrac, B., G. Laubacher, and R. Marocco, Geologie des Andes Peruviennes, *Trav. Doc. ORSTOM*, *122*, 1980.

Emerson, J. D., and M. A. Stoto, Transforming data, in *Understanding Robust and Explanatory Data Analysis*, edited by D. C. Hoaglin, F. Mosteller, and J. W. Tukey, John Wiley, New York, 1983.

Emerson, J. D., and J. Strenio, Boxplots and batch comparison, in *Understanding Robust and Explanatory Data Analysis*, edited by D. C. Hoaglin, F. Mosteller, and J. W. Tukey, John Wiley, New York, 1983.

Ghuman, B. S., and R. Lal, Effects of deforestation on soil properties and microclimate of a high rainforest in southern Nigeria, in *The Geophysiology of Amazonia*, edited by R. E. Dickinson, John Wiley, New York, 1987.

Goodall, C., Examining residuals, in *Understanding Robust and Explanatory Data Analysis*, edited by D. C. Hoaglin, F. Mosteller, and J. W. Tukey, John Wiley, New York, 1983.

Gross, A. M., Confidence interval robustness with long-tailed symmetric distributions, *J. Am. Stat. Assoc.*, *71*, 409–416, 1976.

Guizado, J., Las molasas del Plioceno-Cuaternario del Oriente Peruano, *Bol. Soc. Geol. Peru*, *45*, 5–44, 1975.

Hoaglin, D. C., Letter values: A set of selected order statistics, in *Understanding Robust and Explanatory Data Analysis*, edited by D. C. Hoaglin, F. Mosteller, and J. W. Tukey, John Wiley, New York, 1983.

Hoaglin, D. C., Using quantiles to study shape, in *Exploring Data Tables, Trends, and Shapes*, edited by D. C. Hoaglin, F. Mosteller, and J. W. Tukey, John Wiley, New York, 1985.

Hoaglin, D. C., F. Mosteller, and J. W. Tukey, Introduction to more refined estimators, in *Understanding Robust and Explanatory Data Analysis*, edited by D. C. Hoaglin, F. Mosteller, and J. W. Tukey, John Wiley, New York, 1983.

Huber, P. J., Robust estimation of a location parameter, *Ann. Math. Stat.*, *35*, 73–101, 1964.

Iglewicz, B., Robust scale estimators and confidence intervals for location, in *Understanding Robust and Explanatory Data Analysis*, edited by D. C. Hoaglin, F. Mosteller, and J. W. Tukey, John Wiley, New York, 1983.

Klute, A., and C. Dirksen, Hydraulic conductivity and diffusivity: Laboratory measurements, in Methods of Soil Analysis, Part 1, 2nd ed., edited by A. Klute, *Agronomy*, *9*, 687–734, 1986.

Koch, E., Unos apuntes sobre la geomorphologia del rio Ucayali, *Bol. Soc. Geol. Peru*, *34*, 32–41, 1959.

Kummel, B., Geological reconnaissance of the Contamana region, Peru, *Bull. Geol. Soc. Am.*, *59*, 1217–1262, 1948.

Martinez, J., and B. Iglewicz, A test for departure from normality based on a biweight estimate of scale, *Biometrika*, *68*, 331–333, 1981.

McGill, R., J. W. Tukey, and W. A. Larsen, Variations of boxplots, *Am. Stat.*, *32*(1), 12–16, 1978.

Mosteller, F., and J. W. Tukey, *Data Analysis and Regression*, Addison-Wesley, Reading, Mass., 1977.

Nielsen, D. R., J. H. Biggar, and K. T. Erh, Spatial variability of field-measured soil-water properties, *Hilgardia*, *42*(7), 215–259, 1973.

Oficina Nacional de Evaluación de Recursos Naturales, Inventario y evaluacion semidetallada de los recursos naturales de la zona del Rio Pichis (Proyecto Pichis-Palcazu), Lima, Peru, 1981.

Räsanen, M. E., J. S. Salo, and R. J. Kalliola, Fluvial perturbance in the western Amazon Basin: Regulation by long-term subandean tectonics, *Science*, *238*, 1398–1401, 1987.

Rogowski, A. S., Watershed physics: Soil variability criteria, *Water Resour. Res.*, *8*(4), 1015–1023, 1972.

Rosenberger, J. L., and M. Gasko, Comparing location estimators: Trimmed means, median, and trimean, in *Understanding Robust and Explanatory Data Analysis*, edited by D. C. Hoaglin, F. Mosteller, and J. W. Tukey, John Wiley, New York, 1983.

Ruegg, W., La depresion del Ucayali y Amazonas Superior, *Rev. Assoc. Geol. Argent.*, *7*(2), 106–124, 1952.

SAS Institute, Inc., *SAS Language Guide for Personal Computers*, release 6.03 ed., Cary, N. C., 1988*a*.

SAS Institute, Inc., *SAS Procedures Guide*, release 6.03 ed., Cary, N. C., 1988*b*.

Soil Survey Staff, *Soil Taxonomy*, *USDA Handb. Ser.*, vol. 436, U.S. Government Printing Office, Washington, D. C., 1975.

Spaans, E. J. A., J. Bouma, A. Lansu, and W. G. Wielemaker, Measuring soil hydraulic properties after clearing of tropical rain forest in a Costa Rican soil, *Trop. Agric. Trinidad*, *67*(1), 61–65, 1990.

Tukey, J. W., *Exploratory Data Analysis*, Addison-Wesley, Reading, Mass., 1977.

UNESCO, Tropical forest ecosystems: A state-of-knowledge report, Paris, 1978.

Velleman, P. F., and D. C. Hoaglin, *Applications, Basics, and Computing of Exploratory Data Analysis*, Duxbury Press, Boston, Mass., 1981.

Vidal, J. P., *Geografia del Peru*, Promoción Editorial Inca, Lima, Peru, 1987.

K. Cassel, Department of Soil Science, North Carolina State University, Raleigh, NC 27607.

J. Castro, Proyecto Suelos Tropicales, Aportado 248, Lima 100, Peru.

H. Elsenbeer, Section of Soil Science, Institute of Geography, University of Berne, Hallerstrasse 12, CH-3012 Berne, Switzerland.

(Received September 17, 1991;
revised July 23, 1992;
accepted July 24, 1992.)